Robust fault diagnosis of wind turbines based on MANFIS and zonotopic observers

Esvan-Jesús Pérez-Pérez [a,b], Vicenç Puig [b], Francisco-Ronay López-Estrada [a,*], Guillermo Valencia-Palomo [c], Ildeberto Santos-Ruiz [a], Gloria Osorio-Gordillo [d]

[a] Tecnológico Nacional de México, I.T. Tuxtla Gutiérrez, TURIX-Dynamics Diagnosis and Control Group, Carretera Panam. km 1080, CP 29050, Tuxtla Gutiérrez, Chiapas, Mexico
[b] Universitat Politècnica de Catalunya, Institut de Robòtica i Informàtica Industrial, CSIC-UPC. Parc Tecnològic de Barcelona, C Llorens i Artigas 4-6, 08028, Barcelona, Spain
[c] Tecnológico Nacional de México, I.T. Hermosillo, Av. Tecnológico 115, 83170, Hermosillo, Mexico
[d] Tecnológico Nacional de México, Centro Nacional de Investigación y Desarrollo Tecnológico, Interior Internado Palmira S/N, Col. Palmira, Cuernavaca, Mexico

ARTICLE INFO

Keywords:
Robust fault diagnosis
Takagi–Sugeno observer
Zonotope
MANFIS
ANFIS
Wind-Turbine

ABSTRACT

Wind turbines have become one of the essential sources of energy generation due to their contribution to energy security, economic development, job creation, and technological innovation. This work proposes a methodology for designing robust fault diagnosis systems based on a bank of zonotopic state estimators built upon Takagi–Sugeno (TS) models. The TS models with associated parametric uncertainty are obtained using a Multiple Output Adaptive Neuro-fuzzy Inference System (MANFIS), an extended and improved version of single-input, single-output ANFIS. Its main difference is its multi-output architecture, which allows generalized weighting functions to be obtained, reducing training times, uncertainties estimation, and reduced complexity. As a result, a set of Linear Matrix Inequalities is obtained with the $\mathcal{H}_\infty$ criterion to adjust the parameter of the zonotopic estimator considering the modeling uncertainty. Overall, the work contributes to improving the safety of WT through diagnostic methods that improve its operability. A well-known certified reference case study of a wind turbine system is considered to validate the proposed method.

1. Introduction

Over the past few years, many countries have gradually adopted renewable energy sources, such as wind power, to reduce their reliance on hydrocarbons. According to the Global Wind Energy Council, the installation of wind farms worldwide exceeded 77.6 [GW] in 2022, resulting in a total global capacity increase of over 906 [GW] (Statistics GWEC, 2023). This marks a significant milestone in the history of wind energy and presents a major management challenge for both new and existing wind turbines. Like any electromechanical system, they are prone to faults due to their operational complexity and their exposure to harsh conditions in nature in coasts or mountain environments where they are exposed to turbulent winds. The main objective of efficient electric power generation through wind turbines is the monitoring and diagnosis of the overall system, anticipating serious faults (Liu & Zhang, 2020). Therefore, the task of a fault diagnosis (FD) is to anticipate and prevent a serious fault (Li et al., 2020). The fault diagnosis community has proposed different methods used by energy companies to trigger alarms in response to potential faults (McMorland et al., 2022).

FD methods can be classified into two groups: model-based and data-driven. The first group includes techniques based on differential equations describing the system behavior. According to this model, it is possible to generate residuals and thus detect and isolate faults (Song & He, 2022). On the other hand, data-driven methods use measured data without an explicit mathematical model (Rahimilarki et al., 2019). Generally based on statistical methods (Zhang et al., 2021), and recently on artificial intelligence such as neural networks (Liang et al., 2022), and others. Data-driven depends on the quality and availability of the system information provided by sensors. Most techniques also require historical and large volumes of data for the learning process, reducing their practical applicability. In both cases, robustness is essential to consider the influence of uncertainties, disturbances, and measurement noise, which makes their application more difficult.

Various robust FD schemes have been proposed to minimize the effects of uncertainty, modeling mismatches, disturbances, and measurement noise, such as unknown input observer, descriptor observers

* Corresponding author.
E-mail addresses: esvan.de.jesus.perez@upc.edu (E.-J. Pérez-Pérez), vicenc.puig@upc.edu (V. Puig), frlopez@ittg.edu.mx (F.-R. López-Estrada), gvalencia@hermosillo.tecnm.mx (G. Valencia-Palomo), ildeberto.dr@tuxtla.tecnm.mx (I. Santos-Ruiz), gloria.og@cenidet.tecnm.mx (G. Osorio-Gordillo).

systems (Bougatef et al., 2020), sliding mode observers (Barboni et al., 2022), $\mathcal{H}_\infty$ observers (Sato & Marcos, 2020), adaptive observers (Su et al., 2022), among others. Uncertainties are usually considered unknown but bounded. This assumption has been taken as an advantage for some schemes such as interval observers, zonotopes, and ellipsoids, among others (Wang, Puig, Xu, & Cembrano, 2019). This work will consider the approach based on zonotopes.

For instance, Wang, Puig, Cembrano, and Zhao (2021) presents the design of zonotopic observers for fault detection in linear parameter-varying descriptor systems; noise and disturbance are unknown but limited by zonotopes. Wang et al. (2021b) investigated a zonotopic observer design method for FD in linear parameter-varying systems, based on $\mathcal{H}_\infty$ to ensure residual robustness and reduce false detection. Recently, Pourasghar et al. (2022) addressed the design of zonotopic observers for Takagi–Sugeno systems affected by uncertainty. As discussed, zonotopes are generally used as geometric sets to bound the uncertainties. Under this set-based scheme, robustness to uncertainties and sensitivity to faults is achieved by evaluating the consistency between measurements and estimated states. Nevertheless, these methods require accurate and well-calibrated dynamic models.

In Chen et al. (2013), a fault diagnosis method is proposed that focuses on the use of an ANFIS algorithm based on a priori knowledge of faults by analyzing wind turbine SCADA data. Although it addresses explicitly only electric pitch faults, it provides valuable insights into fault diagnosis techniques. The work by Rajabi et al. (2022) focuses on fault diagnosis for rotating machines and utilizes a multi-output neuro-fuzzy classifier with permutation entropy for signal analysis. The work by Liu et al. (2023) presents a fault detection method based on convolutional deep residual networks using SCADA data. The network proposes to provide accurate fault classification based on raw data. Zhang et al. (2023) propose a scheme for faults diagnosis of bearing in the transmission system through a semi-supervised approach and fusion of vibration and acoustic information. A coupled convolutional residual network is used for discriminative feature extraction, and an enhanced mix-match algorithm performs semi-supervised fault diagnosis. Sun et al. (2023) developed a matching contrastive learning strategy for wind turbine fault diagnosis using unbalanced SCADA data; spatial and temporal characteristics of the data are extracted with a convolutional neural network, then a classifier is trained to identify faults. The reference by Pérez-Pérez et al. (2022) corresponds to our previous contribution and serves as an important point of comparison. While their work utilizes an ANFIS and an interval observer for fault diagnosis, our proposed method incorporates a MAMFIS and a zonotopic observer. The inclusion of the MAMFIS enables the detection of multiple fault types, and the zonotopic observer enhances robustness against disturbances, sensor noise, and model mismatches.

This work introduces a hybrid strategy for robust fault diagnosis in complex systems, leveraging data-driven techniques combined with uncertain Takagi–Sugeno zonotopic observers. The structural analysis employs the graph of a wind turbine process, which generates model structures (MS) without knowledge of a mathematical model. The MS is identified with a Multi-output Adaptive Neuro-Fuzzy Inference System (MANFIS) that can remarkably capture the inherent complexity and nonlinear relationships in wind turbine data. The MANFIS combines the strengths of neural networks and fuzzy systems, making it suitable for system identification. One notable advantage of our proposal is that the MANFIS is trained with only fault-free data, which sets it apart from other approaches that typically require prior knowledge of faulty models. This aspect is crucial as it eliminates the need to label faulty data manually. Instead, fault-free training enables the system to learn healthy operational behavior, allowing for more efficient and accurate fault diagnosis. Each MS identified with the MANFIS is expressed by Takagi–Sugeno models that capture wind turbines' dynamic and nonlinear behavior. Then, a set of robust zonotopic observers is designed to generate residual signals that detect abnormal behaviors on the MSs, detecting and isolating faults. The main advantage of considering zonotopic observers is the inclusion of adaptive thresholds contributing to more precise fault diagnosis and robustness. The observer gains are computed based on sufficient conditions given by a Linear Matrix Inequalities (LMIs) set with $\mathcal{H}_\infty$ performance, which mitigate the effects of uncertainty and disturbance. Finally, simulations of a certified wind turbine benchmark are executed in realistic settings to demonstrate the effectiveness of the proposed method in various fault scenarios. The main contributions of this work can be listed as follows:

- Identification of uncertain TS models using MANFIS and structural analysis using a wind turbine process graph: Uncertain TS models are identified using MANFIS trained on healthy data. Furthermore, taking advantage of the graph-based structural analysis of a wind turbine process to improve understanding of the structural interconnections of the system without the need for a mathematical model.
- Design of TS zonotope observers for the robust detection of faults in the wind turbine. These observers use the identified TS models and take advantage of zonotope representations to effectively monitor and diagnose system behavior under fault conditions in the presence of uncertainty and measurement noise.
- Implementation of a fault isolation stage that uses fault signal matrices. This module enhances diagnostic capabilities by providing identification of specific faults in the wind turbine.

This document is organized as follows: Section 2 presents the preliminaries regarding notation and zonotopes; Section 3 provides an overview of the proposed approach and the derivation of structural models from a process graph; Section 4 describes system identification using MANFIS; Section 5 presents the robust TS zonotopic observers design for fault diagnosis; next, Section 6 presents the results and discussions of MANFIS learning and the fault diagnosis of the wind turbine; finally, Section 7 presents the conclusions.

2. Preliminaries and definitions

In this paper, $\mathbb{R}$ and $\mathbb{N}$ denote the set of real and natural numbers, respectively. $\mathbb{R}^m$ denotes the set of m-dimensional real vectors. $\|\cdot\|_F$ indicates the Frobenius norm, $\|\cdot\|_p$ indicates the p-norm, and $\|\cdot\|_\infty$ indicates the infinity norm.

Definition 2.1 (*Zonotopes Le et al., 2013*)**.** A zonotope $\langle c, R\rangle \subset \mathbb{R}^m$ with center $c \in \mathbb{R}^m$ and generator $R \in \mathbb{R}^{m\times p}$ is a symmetric polytope defined as the affine transformation of a unitary hypercube $[-1, 1]^p \subset \mathbb{R}^p$, s.t., $\langle c, R\rangle = \{c + R\varsigma : \|\varsigma\|_\infty \leq 1\}$.

Definition 2.2 (*Centered Zonotope Combastel, 2003*)**.** A centered zonotope is defined as $\langle R\rangle = \langle 0, R\rangle \subset \mathbb{R}^m$. Any permutation of the columns of R the zonotope remains invariant.

Property 2.1 (*Zonotope Inclusion Alamo et al., 2005*)**.** *Given a zonotope $\mathcal{Z} = \langle c, R\rangle \subset \mathbb{R}^m$, with a vector $c \in \mathbb{R}^m$ and interval matrix $R \in \mathbb{R}^{m\times n}$ denoting the shape of the zonotope, a zonotope inclusion indicated by $\diamond(\mathcal{Z})$ is defined as $\diamond(\mathcal{Z}) = \langle c, [mid(R),\ S]\rangle$, where S is a diagonal matrix that satisfies $S_{\varrho\varrho} = \sum_{\varpi}^{m} \frac{diam(R_{\varrho\varpi})}{2}, \varrho = 1, 2, \ldots, n$, where $mid(\cdot)$ and $diam(\cdot)$ are the center and diameter of interval matrix, respectively.*

Property 2.2. *Representing the Minkowski sum and the linear image as $\oplus$ and $\odot$, respectively, s.t., M is a matrix of appropriate dimension, then, $\langle c_1, R_1\rangle \oplus \langle c_2, R_2\rangle = \langle c_1 + c_2, [R_1, R_2]\rangle$, and $M \odot \langle c, R\rangle = \langle Mc, MR\rangle$.*

3. Overview of the proposed approach

3.1. Wind turbine case study

A benchmark wind turbine, certified for its reliability, is utilized to demonstrate the proposed method. This benchmark is constructed using

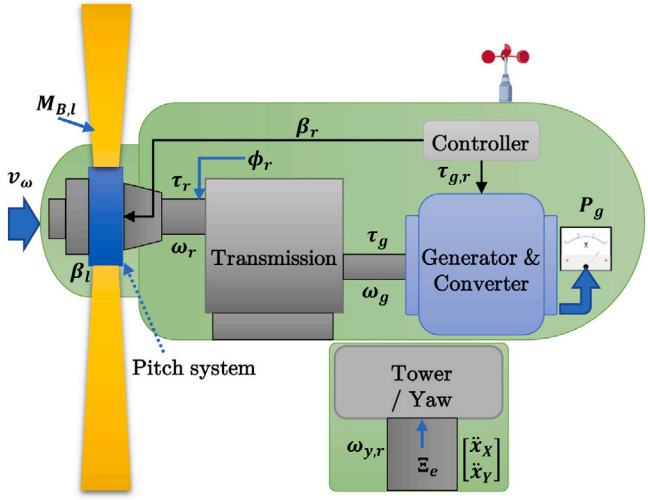

Fig. 1. Wind turbine scheme of components and sensors.

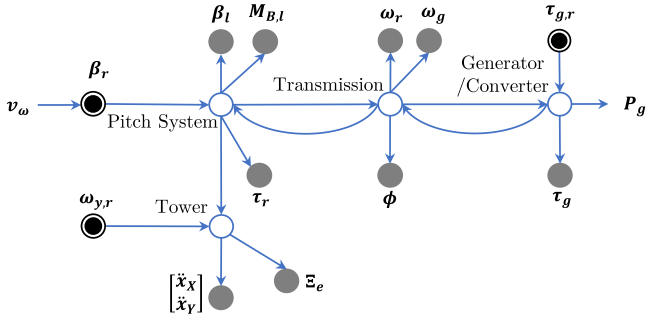

Fig. 2. Graph of a process for the wind turbine.

the Fatigue, Aerodynamics, Structures, and Turbulence (FAST) simulator,[1] a creation of the National Renewable Energy Laboratory (Odgaard & Johnson, 2013). The scientific community has widely accepted this simulator to create and test new control and fault diagnosis systems (Zare & Ayati, 2021).

Fig. 1 shows the schematic diagram of the wind turbine considered as a case study. The turbulent wind input v_w is generated by TurbSim[2] in the simulator. The pitch is related to the three-blade angle variables β_l, where $l = 1, 2, 3$; the root moment $M_{B,l}$; and gets the reference β_r from the controller. The transmission system has the generator τ_g and rotor τ_r torque as input. The outputs are the rotor ω_r and generator ω_g angular velocities; in addition, in the low-speed axis, an azimuth angle sensor ϕ_m is placed. The electrical energy P_g is given by the generator/converter determined by the torque reference $\tau_{g,r}$. The tower is equipped with the signal of yaw reference $\omega_{y,r}$; a sensor that collects the acceleration provided by the wind $\left[\ddot{x}_X \quad \ddot{x}_Y\right]^T$, and another sensor to capture the yaw error Ξ_e. From these relationships, the graph process of the wind turbine can be generated as shown at the bottom of Fig. 2.

3.2. Proposed approach

Model structures (MS) obtained from the graph of a process (GP) describes the relationships between the variables and components of the system (Sztyber et al., 2015). Each MS could be used to generate a residual in a fault diagnosis scheme; the main advantage of using MS is that it does not require knowledge of the mathematical model, unlike other structural analysis methods, such as analytical redundancy relations (Perez-Zuniga et al., 2022), which relate known variables (measured) to model equations.

For the wind turbine, the MSs are constructed by analyzing the graph displayed in Fig. 2 that represents the connections of the wind turbine components and influences variables. All these model structures are shown in Table 1; each MS generates a residual for fault diagnosis. A data-based model is required to construct the residuals given in Table 1. In this work, these models are obtained by an identification process carried out by a MANFIS algorithm, as detailed below.

To generate such residuals, the proposed scheme is presented in Fig. 3. Uncertain TS convex systems are obtained for each variable using MANFIS, using only data from sensors in the wind turbine. Then, a bank of TS zonotopic observers is designed for fault detection through adaptive thresholds of the residuals that compare the consistency between the measured $\mathcal{X}_k^{y_k}$ and estimated $\hat{\mathcal{X}}_k^{zo}$ sensor data. Then, a fault signal matrix that relate residuals with faults is used for fault isolation.

[1] https://www.nrel.gov/wind/nwtc/fast.html
[2] https://www.nrel.gov/wind/nwtc/turbsim.html

4. TS MS identification using MANFIS

Neuro-fuzzy methods combine the benefits of Artificial Neural Networks (ANN) and fuzzy inference systems to approximate dynamic behaviors (Takagi & Sugeno, 1985). For this work, MANFIS is used, which is an improved multi-output version of ANFIS (Benmiloud, 2010). MANFIS produces a weighted sum of linear models from an ANN composed of antecedent and consequent parts. Subsequently, backpropagation and recursive least squares learning are combined to obtain the corresponding neuro-fuzzy hyper-parameters for each network part. To illustrate the procedure, the MANFIS depicted in Fig. 4 structures the convex TS model to estimate the variable $\hat{\omega}_g$. The input vector ζ is made up of the variable estimates $\hat{\omega}_g$ of MS7 from Table 1 as:

$$\zeta = \left[\begin{array}{ccccc} \omega_g(k) & \omega_g(k-1) & \omega_g(k-2) & \tau_g(k) & \tau_r(k) \end{array}\right]^T. \tag{1}$$

The MANFIS estimates the dynamic of each MS and is represented by convex TS systems. Its main strength is that the data sets for the learning stage are constituted of fault-free sensor data, unlike traditional ANN techniques that need faulty data to learn the fault–caused anomalous behavior. The input data for MANFIS are composed of each MS in Table 1 and are built as follows:

Layer 1: Premise layer where the input is assigned to the fuzzy rules and their respective membership function (MF). Each MF, denoted by $\eta(\cdot)$, has three neuro-fuzzy parameters (a_{mo}, b_{mo}, c_{mo}), and is defined as:

$$\breve{\mathcal{O}}^1 = \eta_{mo}(\zeta_o) = \frac{1}{1 + \frac{\zeta_o - c_{mo}}{a_{mo}}^{2b_{mo}}}, \quad \forall m = 1, \ldots, N_{MF}, \quad \forall o = 1, \ldots, N_\zeta, \tag{2}$$

Layer 2: This layer produces the rules by using the preceding MF;

$$\breve{\mathcal{O}}^2 = \mu_i(\zeta) = \prod_{o=1}^{N_\zeta} \eta_{mo}(\zeta_o), \quad \forall i = 1, \ldots, N_v. \tag{3}$$

Each premise parameter ζ_o is calculated and varies in a defined interval $\zeta_o \in \left[\underline{\zeta_o}, \overline{\zeta_o}\right] \subset \mathbb{R}$.

Layer 3: The triggering intensity of each rule is normalized:

$$\breve{\mathcal{O}}^3 = \bar{\mu}_i(\zeta) = \frac{\mu_i(\zeta)}{\sum_{i=1}^{N_v} \mu_i(\zeta)}, \quad \forall i = 1, \ldots, N_v. \tag{4}$$

Layer 4: So-denominated the fuzzy if-then rules of TS are used (Takagi & Sugeno, 1985):

$$\begin{array}{l} \mathcal{R}_i : IF \quad \zeta_1 \quad is \quad \eta_{m1} \quad AND, \ldots, AND \quad \zeta_{N_\zeta} \quad is \quad \eta_{mN_\zeta} \\ \left.\begin{array}{ll} & \breve{\mathcal{O}}^4 = \bar{\mu}_i \xi_i = \bar{\mu}_i(\zeta p_i^I + h_i^I) \\ THEN & \breve{\mathcal{O}}^{4I} = \bar{\mu}_i \xi_i^I = \bar{\mu}_i(\zeta p_i^{II} + h_i^{II}) \\ & \breve{\mathcal{O}}^{4II} = \bar{\mu}_i \xi_i^{II} = \bar{\mu}_i(\zeta p_i^{III} + h_i^{II}) \end{array}\right\}, \quad \forall i = 1, \ldots, N_v. \end{array} \tag{5}$$

Table 1
Model structures of wind turbine.

Pitch system	
MS1	$r_1 = \beta_1(k) - \hat{\beta}_1(k)(\beta_1(k), \beta_1(k-1), \beta_1(k-2), \beta_r(k), \beta_r(k-1))$
MS2	$r_2 = \beta_2(k) - \hat{\beta}_2(k)(\beta_2(k), \beta_2(k-1), \beta_2(k-2), \beta_r(k), \beta_r(k-1))$
MS3	$r_3 = \beta_3(k) - \hat{\beta}_3(k)(\beta_3(k), \beta_3(k-1), \beta_3(k-2), \beta_r(k), \beta_r(k-1))$
MS4	$r_4 = M_{B,1}(k) - \hat{M}_{B,1}(k)(M_{B,1}(k), M_{B,1}(k-1), M_{B,1}(k-2), \beta_r(k), \beta_r(k-1)),$
MS5	$r_5 = M_{B,2}(k) - \hat{M}_{B,2}(k)(M_{B,2}(k), M_{B,2}(k-1), M_{B,2}(k-2), \beta_r(k), \beta_r(k-1)),$
MS6	$r_6 = M_{B,3}(k) - \hat{M}_{B,3}(k)(M_{B,3}(k), M_{B,3}(k-1), M_{B,3}(k-2), \beta_r(k), \beta_r(k-1)),$
Transmission	
MS7	$r_7 = \omega_r(k) - \hat{\omega}_r(\omega_r(k), \omega_r(k-1), \omega_r(k-2), \tau_g(k), \tau_r(k))$
MS8	$r_8 = \omega_g(k) - \hat{\omega}_g(\omega_g(k), \omega_g(k-1), \omega_g(k-2), \tau_g(k), \tau_r(k))$
MS9	$r_9 = \phi_r(k) - \hat{\phi}_r(k)(\phi_r(k), \phi_r(k-1), \phi_r(k-2), \omega_r(k), \omega_r(k-1))$
Yaw system	
MS10	$r_{10} = \Xi_e(k) - \hat{\Xi}_e(k)(\Xi_e(k), \Xi_e(k-1), \Xi_e(k-2), \omega_{yr}(k), \omega_{yr}(k-1))$
MS11	$r_{11} = \ddot{x}_X(k) - \hat{\ddot{x}}_X(k)(\ddot{x}_X(k), \ddot{x}_X(k-1), \ddot{x}_X(k-2), \omega_{yr}(k), \omega_{yr}(k-1))$
Generator/converter	
MS12	$r_{12} = P_g(k) - \hat{P}_g(k)(P_g(k), P_g(k-1), P_g(k-2), \tau_g(k), \tau_g(k-1), \tau_g(k-2))$
MS13	$r_{13} = \tau_g(k) - \hat{\tau}_g(k)(\tau_g(k), \tau_g(k-1), \tau_g(k-2)\tau_{gr}(k), \tau_{gr}(k-1))$

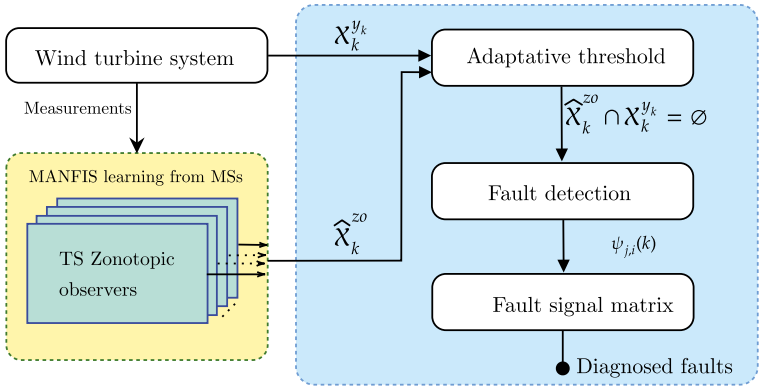

Fig. 3. Scheme of the proposed method for fault diagnosis.

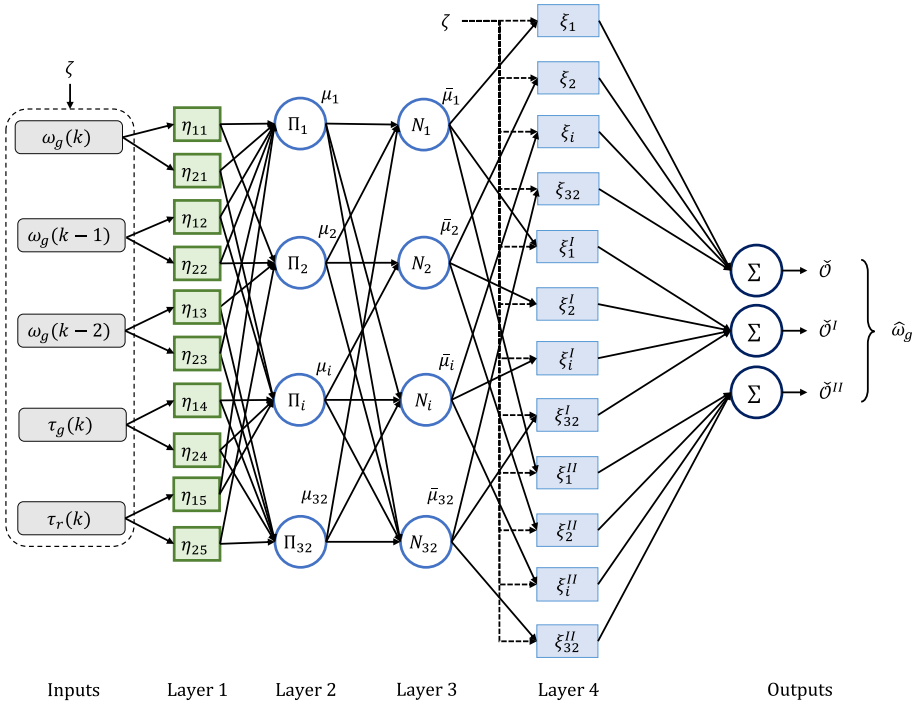

Fig. 4. Polytopic TS learning scheme for ω_g.

Output: This layer calculates the total output $\mathcal{O}^5$ by adding up all the information from layer four.

$$\check{\mathcal{O}}^5 = \sum_{i=1}^{N_v} \bar{\mu}_i \xi_i, \tag{6}$$

$$\check{\mathcal{O}}^{5I} = \sum_{i=1}^{N_v} \bar{\mu}_i \xi_i^I, \tag{7}$$

$$\check{\mathcal{O}}^{5II} = \sum_{i=1}^{N_v} \bar{\mu}_i \xi_i^{II}. \tag{8}$$

After the MANFIS has been trained and the normalized values (4) and the fuzzy rules (5) have been determined, proceed to build the polytopic TS system. The case of MS8 will be employed for illustrative purposes; it is given in the following terms

$$\hat{\omega}_g = \check{\mathcal{O}}^5 = \sum_{i=1}^{N_v} \bar{\mu}_i(\zeta(k)) \Big(p_{1i}\omega_g(k) + p_{2i}\omega_g(k-1) + p_{3i}\omega_g(k-2) + p_{4i}\tau_g(k) + p_{5i}\tau_r(k) + h_i \Big). \tag{9}$$

Terms in (9) can be rearranged as:

$$\hat{\omega}_g = \sum_{i=1}^{N_v} \bar{\mu}_i(\zeta(k)) \left(\overbrace{\begin{bmatrix} p_{1i}^1 & p_{2i}^1 & p_{3i}^1 \\ p_{1i}^2 & p_{2i}^2 & p_{3i}^2 \\ p_{1i}^3 & p_{2i}^3 & p_{3i}^3 \end{bmatrix}}^{A_i} x + \overbrace{\begin{bmatrix} p_{4i}^1 & p_{5i}^1 \\ p_{4i}^2 & p_{5i}^2 \\ p_{4i}^3 & p_{5i}^3 \end{bmatrix}}^{B_i} u + \overbrace{\begin{bmatrix} h_i^1 \\ h_i^2 \\ h_i^3 \end{bmatrix}}^{h_i} \right), \tag{10}$$

where $x = \begin{bmatrix} \omega_g(k) & \omega_g(k-1) & \omega_g(k-2) \end{bmatrix}^T$ is the state vector and $u = \begin{bmatrix} \tau_g & \tau_r \end{bmatrix}^T$ is the input vector; the superscript $\iota = 1, 2, 3$ indicates the number for output for MAMFIS, such as the system described in (11) is obtained.

$$x(k+1) = \sum_{i=1}^{N_v} \bar{\mu}_i(\zeta(k)) \left(A_i x(k) + B_i u(k) + h_i \right),$$
$$y(k) = Cx(k), \tag{11}$$

where N_v is obtained by $N_v = \left(N_{MF}\right)^{N_\zeta}$, $\bar{\mu}_i(\zeta(k))$ denotes the premise functions, $A_i \in \mathbb{R}^{n_x \times n_x}$, $B_i \in \mathbb{R}^{n_x \times n_u}$, $h_i \in \mathbb{R}^{n_x}$, and $C \in \mathbb{R}^{n_y \times n_x}$ indicates the system matrices, and $y(k) \in \mathbb{R}^{n_y}$ represents the output vector that is calculated. Uncertainties related to model mismatches and uncertainty due to aerodynamic loads and sensor noise are included. Matrices ΔA_i and ΔB_i are the uncertainties.

$$x(k+1) = \sum_{i=1}^{N_v} \bar{\mu}_i(\zeta(k)) \left((A_i + \Delta A_i)x(k) + (B_i + \Delta B_i)u(k) + h_i \right) + E_d\, d(k),$$
$$y(k) = Cx(k) + F_v\, v(k), \tag{12}$$

E_d and F_v represents the uncertainty and noise matrices with fixed sizes, $d(k) \in \mathbb{R}^{n_x}$ indicates the uncertainty by aerodynamic loads, and $v(k) \in \mathbb{R}^{n_y}$ indicates the sensor noise. The values of the uncertain matrices are obtained from the error covariance matrix Θ of all consequent parameters, which is generated from the hybrid learning algorithm:

$$\Theta = \begin{pmatrix} \sigma_{11}^2 & \sigma_{12}^2 & \cdots & \sigma_{1j}^2 \\ \sigma_{21}^2 & \sigma_{22}^2 & \cdots & \sigma_{2j}^2 \\ \vdots & \vdots & \ddots & \vdots \\ \sigma_{i1}^2 & \sigma_{i2}^2 & \cdots & \sigma_{ij}^2 \end{pmatrix}, \tag{13}$$

where the elements on the main diagonal, $\sigma_{i,i}^2$, are the variances $\mathrm{var}(c_i)$ obtained at the end of the training; and the elements off the main diagonal, $\sigma_{i,j}^2$, are the covariances $\mathrm{cov}(c_i, c_j)$, $i \neq j$.

To build matrices ΔA_i and ΔB_i, the standard deviations are calculated from the variances extracted from matrix Θ in (13), and are stored in Υ. Subsequently, Υ is reshaped to the appropriate dimensions of matrices A_i and B_i, where:

$$\Upsilon = \begin{bmatrix} \sigma_1 \\ \vdots \\ \sigma_{nm} \end{bmatrix}; \tag{14}$$

$$\Delta A_i = \begin{pmatrix} \sigma_{1i} & \sigma_{2i} & \sigma_{3i} \\ \sigma_{1i}^I & \sigma_{2i}^I & \sigma_{3i}^I \\ \sigma_{1i}^{II} & \sigma_{2i}^{II} & \sigma_{3i}^{II} \end{pmatrix}, \quad \Delta B_i = \begin{pmatrix} \sigma_{4i} & \sigma_{5i} \\ \sigma_{4i}^I & \sigma_{5i}^I \\ \sigma_{4i}^{II} & \sigma_{5i}^{II} \end{pmatrix}. \tag{15}$$

To calculate the disturbances, the following procedure, as in Blesa et al. (2010), is considered; E_d is defined as follows:

$$E_d^\iota = \max(\omega_g - \hat{\omega}_g - \lambda,\ \hat{\omega}_g - \omega_g - \lambda), \tag{16}$$

where λ is a scalar that limits the uncertainty. E_d is a diagonal matrix of suitable sizes constructed as $E_d = \mathrm{diag}([E_d^1, E_d^2, E_d^3])$. F_v is a diagonal matrix of suitable sizes shaped by the additive noise of the sensors in the wind turbine simulator. Vectors $d(k)$ and $v(k)$ are supposed to be unknown but bounded. These convex models are used to design the TS observers as described below.

5. Robust MS evaluation using robust zonotopic TS observers

5.1. Zonotopic TS observer

Let us consider an uncertain TS system (12) subject to disturbances and measurement noises as:

$$x(k+1) = (A_z + \Delta A_z)x(k) + (B_z + \Delta B_z)u(k) + h_z + E_d d(k),$$
$$y(k) = Cx(k) + F_v v(k), \tag{17}$$

where $A_z = \sum_{i=1}^{N_v} \bar{\mu}_i(\zeta(k))A_i$, $\Delta A_z = \sum_{i=1}^{N_v} \bar{\mu}_i(\zeta(k))\Delta A_i$, $B_z = \sum_{i=1}^{N_v} \bar{\mu}_i(\zeta(k))B_i$, $\Delta B_z = \sum_{i=1}^{N_v} \bar{\mu}_i(\zeta(k))\Delta B_i$, $h_z = \sum_{i=1}^{N_v} \bar{\mu}_i(\zeta(k))h_i$.

It is assumed that,

$$\underline{\Delta A_z} \leq \Delta A_z \leq \overline{\Delta A_z}, \tag{18}$$

$$\underline{\Delta B_z} \leq \Delta B_z \leq \overline{\Delta B_z}, \tag{19}$$

where $\underline{\Delta A_z} \in \mathbb{R}^{n_x \times n_x}$, $\underline{\Delta B_z} \in \mathbb{R}^{n_x \times n_u}$, $\overline{\Delta A_z} \in \mathbb{R}^{n_x \times n_x}$, and $\overline{\Delta B_z} \in \mathbb{R}^{n_x \times n_u}$ are matrices containing the minimum and maximum values of ΔA_z and ΔB_z, respectively.

The uncertain parameters can be approximated in a single term according to Chen and Patton (2012). Therefore, (17) is rewritten as follows

$$x(k+1) = A_z x(k) + B_z u(k) + h_z + E_d d(k) + E_\delta \delta(k),$$
$$y(k) = Cx(k) + F_v v(k), \tag{20}$$

with

$$E_\delta \delta(k) = \Delta A_z x(k) + \Delta B_z u(k) \tag{21}$$

where E_δ is the uncertainty distribution matrix of appropriate dimensions and $\delta(k) \in \mathbb{R}^{n_x}$ is a vector that embeds the effect of uncertainty. For example, in a wind turbine, aerodynamic loads and sensors noise are unknown but bounded, such as:

$$\mathcal{D} = \{ d(k) \in \mathbb{R}^{n_x} : |d(k) - c_d| \leq \overline{d}(k),\ c_d \in \mathbb{R}^{n_x}, \overline{d}(k) \in \mathbb{R}^{n_x} \},$$
$$\mathcal{V} = \{ v(k) \in \mathbb{R}^{n_y} : |v(k) - c_v| \leq \overline{v}(k),\ c_v \in \mathbb{R}^{n_y}, \overline{v}(k) \in \mathbb{R}^{n_y} \}, \tag{22}$$

where $c_d, \overline{d}(k), c_v$ and $\overline{v}(k)$ are constant vectors.

This work considers a zonotopic depiction of state estimation, such as (22) is rewritten as follows:

$$\mathcal{D} = \langle c_d, R_d \rangle,$$
$$\mathcal{V} = \langle c_v, R_v \rangle, \tag{23}$$

where c_d and c_v denote the centers of the disturbance and noise-bounding zonotopes, respectively, with their generator matrices $R_d \in \mathbb{R}^{n_x \times n_x}$ and $R_v \in \mathbb{R}^{n_y \times n_y}$, respectively.

For the estimation of the TS system with uncertainty (20), the following zonotopic TS observer is considered:

$$\hat{x}(k+1) = A_z\hat{x}(k) + B_z u(k) + h(k) + L_z(y(k) - \hat{y}(k)),$$
$$\hat{y}(k) = C\hat{x}(k), \tag{24}$$

where $\hat{x}(k+1)$ is the vector of estimated states and $\hat{y}(k)$ is the prediction output. The objective is to find the observer gain matrix such that the estimation error between (20) and (24) converges asymptotically to zero. The goal is to find the observer gain matrix $L_i \in \mathbb{R}^{n_x \times n_y}$, such that the state estimation error between (20) and (24) converges asymptotically to zero, i.e. $e(k) = x(k) - \hat{x}(k)$, whose dynamics error is described by:

$$e(k+1) = (A_z - L_z C)e(k) + E_d d(k) - F_v v(k) + E_\delta \delta(k), \tag{25}$$

An observer that wraps the states corresponding to the system with uncertainty (20), can be obtained as a zonotope $\hat{\mathcal{X}}_k = \langle c_k^x, R_k^x \rangle$ using the observer (24) and Proposition 1 considering the bounded uncertainties and zonotopic representation under the following assumptions.

Assumption 5.1. The uncertainties and disturbances represented in (20) are assumed to be bounded by zonotope centered (see Definition 2.2), i.e., $\forall k \geq 0$, $d = \in [-1,1]^{n_d} = \langle 0, I_{n_d} \rangle$, $v \in [-1,1]^{n_v} = \langle 0, I_{n_v} \rangle$ and $\delta \in [-1,1]^{n_z} = \langle 0, I_{n_z} \rangle$ where I_{n_d}, I_{n_v} and I_{n_z} denote the identity matrix.

Assumption 5.2. The initial state x_0 belongs to the set $\mathcal{X}_0^{zo} = \langle c_{k,0}^{zo}, R_{k,0}^{zo} \rangle$, where $c_{k,0}^{zo} \in \mathbb{R}^{n_x}$ denotes the center and $R_{x,0}^{zo} \in \mathbb{R}^{n_x \times n_{R_{k,0}^{zo}}}$ is a non-empty matrix containing the generators matrix of the initial zonotope $\mathcal{X}_0^{zo}$.

Proposition 1. *With the system (20) and observer (24), the zonotope $\hat{\mathcal{X}}_k^{zo} = \langle c_{k+1}^{zo}, R_{k+1}^{zo} \rangle$ is recursively forward predicted as:*

$$c_{k+1}^{zo} = (A_z - L_z C)c_k^{zo} + B_z u_k + h_k + L_z y_k \tag{26}$$
$$R_{k+1}^{zo} = \begin{bmatrix} (A_z - L_z C)\bar{R}_k^{zo} & E_d & -L_z F_v & E_\delta \end{bmatrix}$$
$$\bar{R}_k^{zo} = \downarrow_q (R_k^{zo}).$$

and the reduction operator $\downarrow_q$ suffices to satisfy $\bar{R}_k = \downarrow_q (R)$, and $\hat{x}(k) \in \langle c_k, R_k \rangle \subset \langle c_k, \bar{R}_k \rangle$, furthermore, the zonotope inclusion Property 2.1 holds for all $k \geq 0$.

Proof. Assuming $\hat{\mathcal{X}}^{zo} = \langle c_{k+1}^{zo}, R_{k+1}^{zo} \rangle$ at instant k (true at $k \geq 0$) and $\downarrow_{q,W}$ has preserved inclusion property, $\hat{\mathcal{X}}^{zo} = \langle c_k, \bar{R}_k \rangle$. Since $d \in \langle 0, I_{nd} \rangle$, $v \in \langle 0, I_{n_v} \rangle$ and $z \in \langle 0, I_{n_z} \rangle$ (20), from (24), it comes:

$$\hat{x}(k+1) = ((A_z - L_z C) \odot \langle c_k^{zo}, R_k^{zo} \rangle) \oplus (B_z \odot \langle u_k, 0 \rangle) \oplus (\langle h_z, 0 \rangle) \tag{27}$$
$$\oplus (L_z \odot \langle y_k, 0 \rangle) \oplus (E_d \odot \langle 0, I_{n_d} \rangle) \oplus (-L_z F_v \odot \langle 0, I_{n_v} \rangle) \oplus (E_\delta \odot \langle 0, I_{n_z} \rangle).$$

Applying the zonotope Property 2.2 obtains (26), hence the proof is fulfilled. □

Note from expression (27) that the terms $\langle h_z, 0 \rangle$, $(B_z \odot \langle u_k, 0 \rangle)$ and $(L_z \odot \langle y_k, 0 \rangle)$ had no impact on the generator matrix R_{k+1}^{zo} and influence only the center matrix c_{k+1}^{zo} of the zonotope $\langle c_{k+1}^{zo}, R_{k+1}^{zo} \rangle$. Taking into account the dynamics of the error (25), the set of zonotopes bounding the estimation error can also be obtained iteratively as

$$e(k+1) \in \langle 0, R_{k+1}^e \rangle \tag{28}$$

where $R_{k+1}^e = \begin{bmatrix} (A_z - L_z C)\bar{R}_k^{zo} & E_d & -L_z F_v & E_\delta \end{bmatrix}$. The main challenge in building the bounding observer is reduce the influence of uncertainties and unknown disturbances. To address this, the $\mathcal{H}_\infty$ criterion technique for designing the observer gain L_z for the zonotopic observer in Proposition 1 is considered. The dynamics of the estimation error (25) is rewritten as follows:

$$e(k+1) = \Phi_z e(k) + \Gamma_z \varphi(k), \tag{29}$$

where $\Phi_z = A_z - L_z C$ and $\Gamma_z = \begin{bmatrix} E_d & F_v & E_\delta \end{bmatrix}, \varphi(k) = \begin{bmatrix} d(k) & v(k) & \delta(k) \end{bmatrix}^T$.

5.2. Zonotopic TS observer design

The following theorem provides sufficient conditions for the estimation of the observer gains and the performance of $\mathcal{H}_\infty$ from the estimation error given in (29).

Theorem 5.1. *The estimation error dynamics in (29) is asymptotically stable with the performance $\mathcal{H}_\infty$, satisfies the condition $\|e(k)\|_2^2 < \gamma^2 \|\varphi(k)\|_2^2$ and attenuation index $\gamma > 0$, with $\bar{\gamma} = \gamma^2$, if there are matrices $P = P^T > 0$ and $L_z, z \in \{1, \ldots, Nv\}$, such that the following optimization problem is satisfied:*

$$min \ -\bar{\gamma}$$

subject to the following LMI:

$$\begin{pmatrix} -P + I & 0 & 0 & 0 & A_z^T P - C^T W_z^T \\ \star & -\bar{\gamma} I & 0 & 0 & E_d^T P \\ \star & \star & -\bar{\gamma} I & 0 & F_v^T - W_z^T \\ \star & \star & \star & -\bar{\gamma} I & E_\delta^T P \\ \star & \star & \star & \star & -P \end{pmatrix} < 0 \tag{30}$$

The observer gains are calculated as $L_z = P^{-1} W_z, z \in \{1, \ldots, Nv\}$, the attenuation index is $\gamma = \sqrt{\bar{\gamma}}$.

Proof. Proof is displayed in the Appendix □

5.3. Fault diagnosis scheme

The MSs ($\hat{y}_s(k)$) of Table 1 are computed by MANFIS; where s refers to the identified variables. All identified variables includes uncertainty and noise in accordance with (22), they are propagated through zonotopic observer; a $\mathcal{X}_k^{y_k}$ strip is calculated regarding every measured variable of $y_s(k)$ as:

$$\mathcal{X}_k^{y_k} = \left\{ x(k) \in \mathbb{R}^{n_x} : \left| Cx(k) - y_s(k) \right| \leq F_\sigma \right\}. \tag{31}$$

Fig. 5 shows the fault detection process by evaluating the zonotopic sets. At each instant k, we evaluate: if $\hat{\mathcal{X}}_k^{zo} \cap \mathcal{X}_k^{y_k} = \emptyset$, then, fault is true. There is no fault if there is an intersection between measurements and estimations.

The evaluation for each MS, when faults exist, produces residuals $r_s(k)$ and these are collected in a fault signal matrix (FSM) which are formed as follows:

$$\psi_{s,j}(k) = \begin{cases} 0 & \text{if} \quad r_s(k) \text{ is congruent (No fault)} \\ 1 & \text{if} \quad r_s(k) \text{ is not congruent (Fault)} \end{cases}, s = 1, \ldots, N_y; \ j = 1, \ldots, N_f. \tag{32}$$

where N_f is the number of fault cases, the isolation is carried under column reasoning, analyzing the FSM and the binary relationship among the activated residuals for every fault. The results of the diagnostic scheme based on MANFIS and zonotopic TS observers are discussed below.

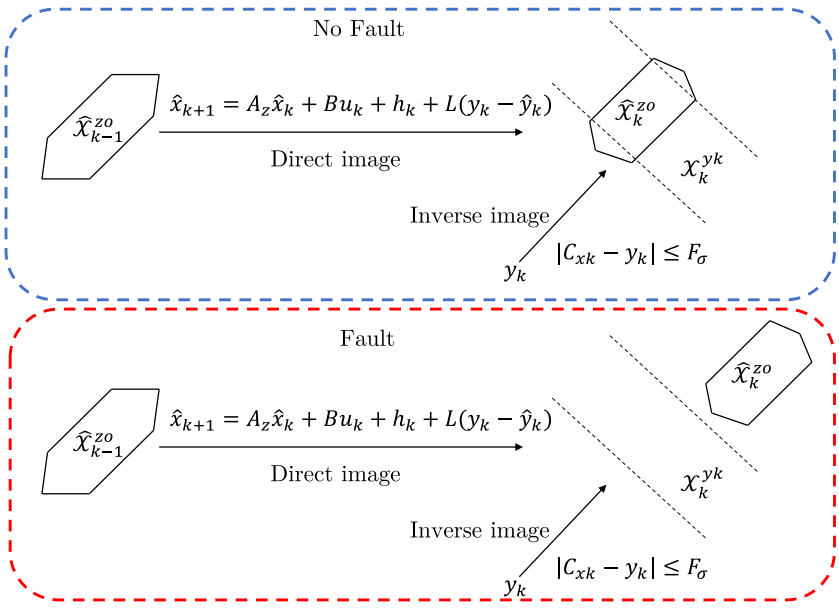

Fig. 5. Graphic interpretation of the fault detection process with zonotopes.

Table 2
Experimental setup.

Attribute	Value
Time of simulation	630 [s]
Sampling rate	80 [Hz]
Samples for each measurement	50401
Subset for training 70%	35281
Subset for test 15%	7560
Subset for validation 15%	7560

6. Results and discussions

This section reveals the outcomes of fault diagnosis achieved in various scenarios delineated for the FAST wind turbine benchmark, as elucidated in Odgaard and Johnson (2013). The Benchmark uses a 5 [MW] three-blade variable speed turbine with full-span pitch control. Its main characteristics are: hub height is 89.6 [m], rotor radius is 63 [m], with a nominal speed of 12.1 [rpm]. TurbSIM, a certified stochastic, full-field turbulence simulator, generates the turbulent wind input. The wind speed averages 17 [m/s] at the shaft height of 90 [m], as shown in Fig. 6. The experimental setup used to obtain the MANFIS training data sets is detailed in Table 2.

Training continues until the RMSE estimation error is as close to zero. Table 3 exhibits the training results for MS. Column 3 presents the number of fuzzy rules corresponding to the premise parameters obtained during the learning processes. The accuracy of MANFIS is quantified using the Root Mean Square Error (RMSE), which can be found in Column 4. The RMSE is calculated using the following equation:

$$\text{RMSE} = \sqrt{\frac{1}{N_\epsilon}\sum_{\epsilon=1}^{N_\epsilon}(y_\epsilon - \hat{y}_\epsilon)^2} \tag{33}$$

where y_ϵ is the real variable, $\hat{y}_\epsilon$ is the identified variable by MANFIS and N_ϵ is the number of registers. During the training process, a maximum of 100 epochs was conducted. The RMSE was computed at the magnitudes of 10^{-3} and 10^{-4}. It was observed that the RMSE did not show a tendency to decrease further beyond these values. This indicates that the MANFIS model with the proposed structures exhibits high accuracy in the identification process.

Multiple simulations were conducted as part of the benchmark to generate a free-faults dataset and establish the structure of the convex

Table 3
RMSE obtained after training.

MS	Estimated variable	Number of fuzzy rules	RMSE
1	$\hat{\beta}_1$	32	9.0876×10^{-3}
2	$\hat{\beta}_2$	32	9.8544×10^{-3}
3	$\hat{\beta}_3$	32	8.9876×10^{-3}
4	$\hat{M}_{B,1}$	32	6.8569×10^{-3}
5	$\hat{M}_{B,2}$	32	7.5813×10^{-3}
6	$\hat{M}_{B,3}$	32	6.3589×10^{-3}
7	$\hat{\omega}_r$	32	4.9851×10^{-4}
8	$\hat{\omega}_g$	32	5.0499×10^{-4}
9	$\hat{\phi}_r$	32	4.5689×10^{-4}
10	$\hat{\Xi}_e$	32	2.9825×10^{-4}
11	$\hat{x}_X$	32	6.7219×10^{-4}
12	$\hat{P}_g$	32	7.2583×10^{-4}
13	$\hat{\tau}_g$	32	3.1268×10^{-4}

TS systems. As an illustration, Fig. 7 illustrates the graph of the TS zonotopic observer representing the $\hat{\omega}_g$ variable. The upper and lower boundaries are denoted by the green and yellow lines, respectively. These bounds are formed by the zonotopic observer encompassing the ω_g variable under fault-free conditions.

Faults in sensors and actuators were induced based on Table 4 to assess the effectiveness of the proposed approach.

- Sensor faults: There are three scaled value faults, where f_1 by a factor of 0.95, f_3 by a factor of 0.95, and f_5 by a factor of 1.1; f_4 by a fixed value of 1, f_2 by an offset of −0.5, and f_6 by a bit error.

- Actuator faults: f_7 and f_8 are pitch faults, referring to air in oil is incipient type and abrupt hydraulic damage. f_9 involves an offset in the control loop of the generator by a constant of 1000 Nm. Finally, f_{10} corresponds to a fixed value of 0 rad/s in the control signal of the Yaw system.

The complete sequence of ten faults presented in Table 4 is applied to verify the proposed fault diagnosis method. As shown in Table 5, the faults detected at the time of occurred were determined using the FSM constructed according to (32). Fault detection and isolation can be realized easily by analyzing the FSM. For example, in Fig. 8, f_3 is observed in the ω_g sensor; the activation period is from 130 [s] to 155 [s], and it can be seen that the fault affects the ω_g signal, which

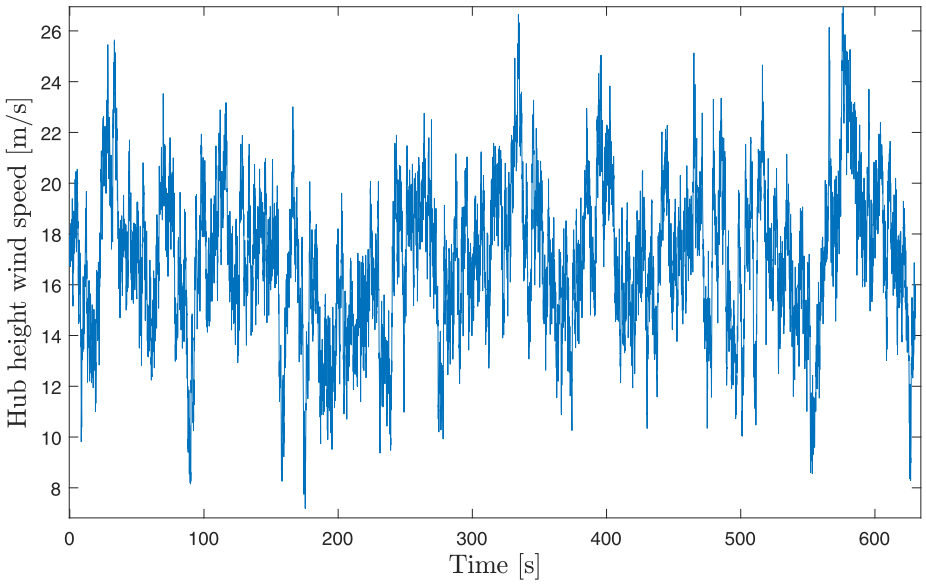

Fig. 6. Wind profile using in simulations generated by TurbSIM.

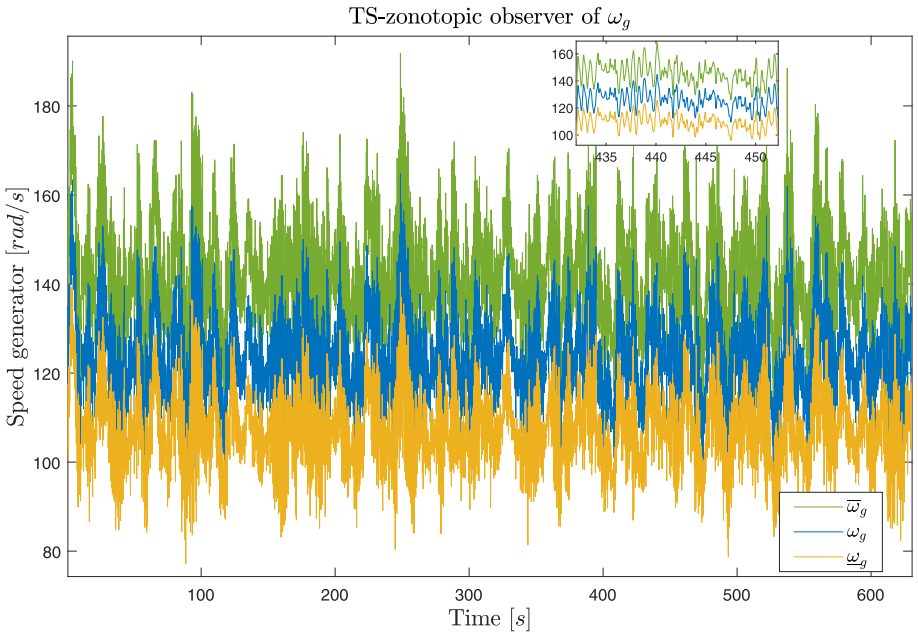

Fig. 7. TS zonotopic observer for ω_g.

Table 4
Faults considered in the wind turbine.

Fault	Description	Time interval [s]
f_1	Fault in sensor $M_{B,2}$	20–45
f_2	Fault in accelerometer sensor $\ddot{x}_X$	75–100
f_3	Fault in sensor ω_g	130–155
f_4	Fault in angle sensor β_1	185–210
f_5	Fault in sensor P_g	240–265
f_6	Fault in encoder ϕ	295–320
f_7	Fault incipient in Pitch actuator	350–410
f_8	Fault abrupt in Pitch actuator	440–465
f_9	Fault in Generator Torque	495–520
f_{10}	Fault in Yaw actuator	550–575

exceeds the upper threshold of the zonotopic observer, the activated residual is r_8 according to the information shown in the incidence matrix. Let us consider the f_4 in the corresponding β_1 sensor from 185 [s] to 210 [s], whose corresponding residuals are shown in Fig. 9; as can be observed, the β_1 signal affected by the fault exceeds the lower threshold of its respective zonotopic observer, the activated residual is r_1 in the incidence matrix. The f_9 in the generator torque τ_g is observed in Fig. 10, the fault was triggered from 495 [s] to 520 [s]; it can be seen that the fault in the actuator affects the τ_g signal, where it exceeds the upper threshold of its zonotopic observer, the activated residual is r_7 in incidence matrix. Then, fault isolation is carried out by analyzing this particular signature with binary logic. A similar analysis can be performed for the rest of the faults.

The proposed method is compared to various FD schemes to assess its effectiveness. Table 6 presents a comparison between the proposed method and preceding works registered in the literature; TSZO denotes the proposed method. The table includes the fault scenarios and compares the time required (TD) for the fault diagnosis system to detect

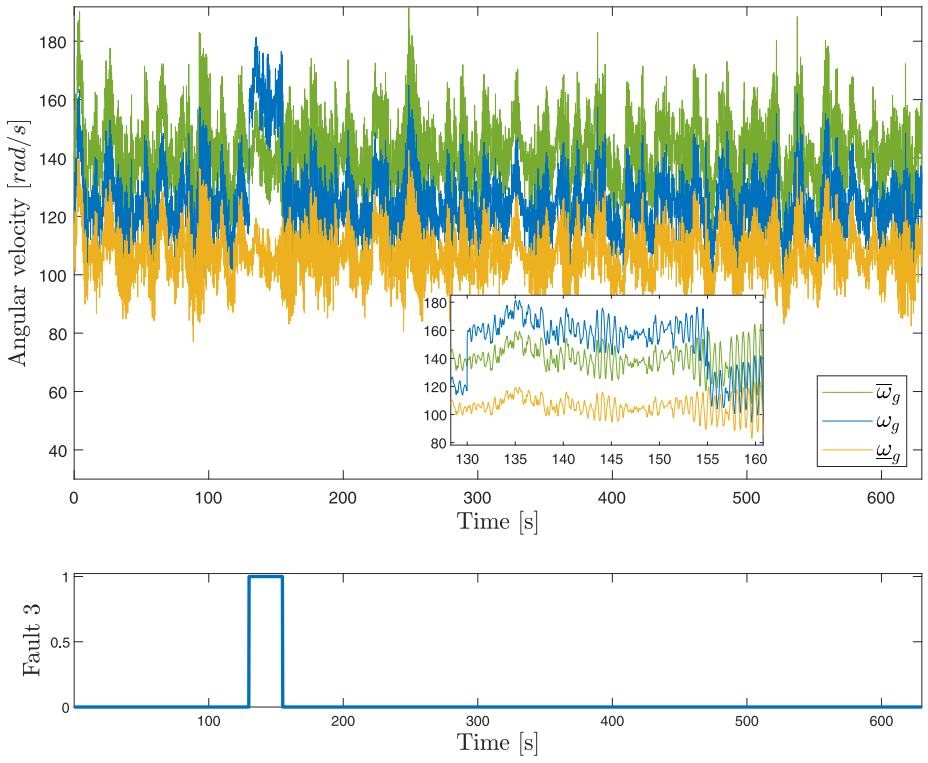

Fig. 8. Detection of f_3 in the sensor of ω_g.

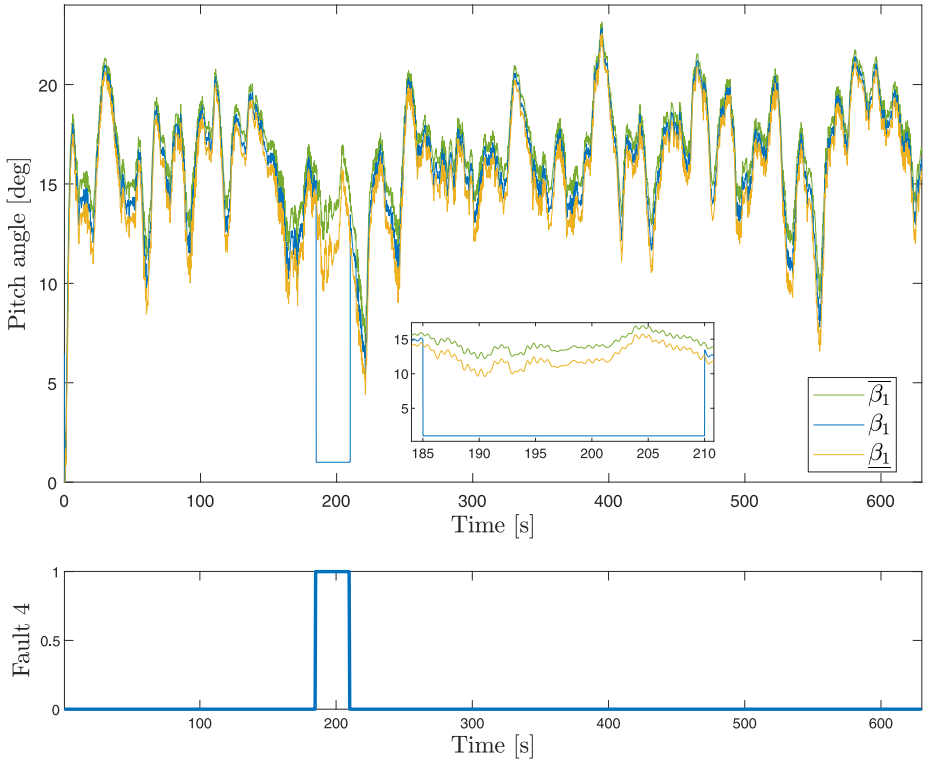

Fig. 9. Detection of f_4 in the sensor of β_1.

the fault. This metric is the most accepted and standard for this kind of approach. As can be seen, the TSZO can detect faults in less time than the other approaches. The last row is a checkmark that compares the robustness criteria to noise and uncertainties. The results obtained from the following FD methods collected from the literature:

- ANN and k-Nearest Neighbors (AKNN) (Pashazadeh et al., 2018): this method combines an ANN and k-NN algorithm for Fault Detection. However, it does not take into account the faults labeled as (NC) f_1 and f_7 in the analysis.

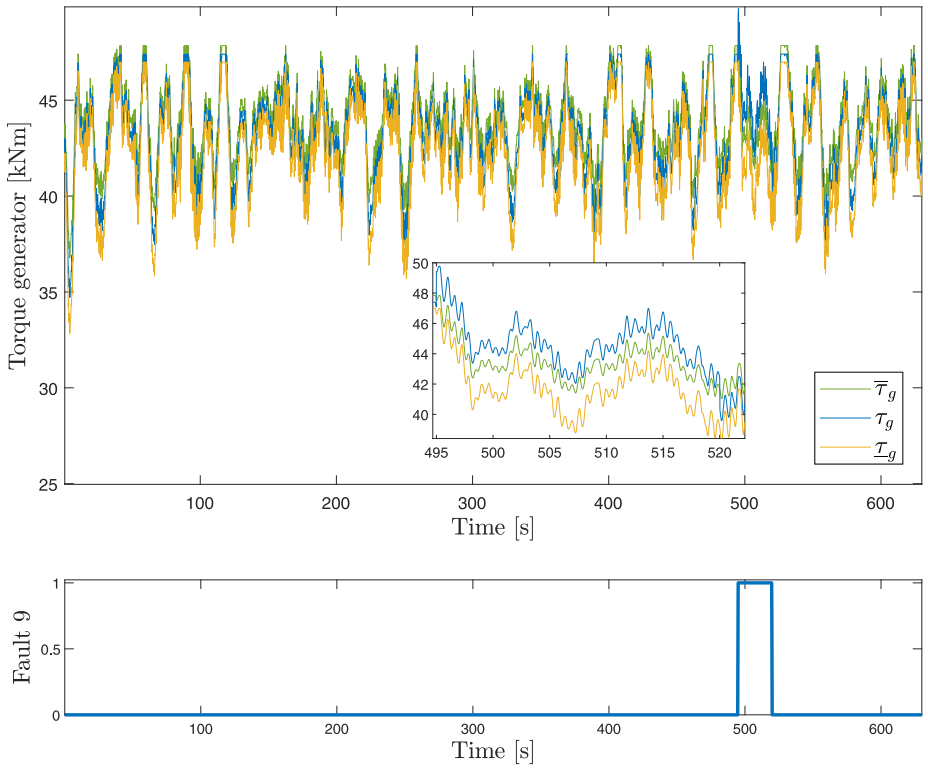

Fig. 10. Detection of f_9 in the Generator Torque τ_g.

Table 5
Fault signal matrix for the set of the different fault scenarios.

FSM	f_1	f_2	f_3	f_4	f_5	f_6	f_7	f_8	f_9	f_{10}
1	0	0	0	1	0	0	1	0	0	0
2	0	0	0	0	0	0	1	0	0	0
3	0	0	0	0	0	0	1	0	0	0
4	0	0	0	0	0	0	0	1	0	0
5	1	0	0	0	0	0	0	1	0	0
6	0	0	0	0	0	0	0	1	0	0
7	0	0	0	0	0	0	0	0	1	0
8	0	0	1	0	0	0	0	0	0	0
9	0	0	0	0	0	1	0	0	0	0
10	0	0	0	0	0	0	0	0	0	1
11	0	1	0	0	0	0	0	0	0	0
12	0	0	0	0	1	0	0	0	0	0
13	0	0	0	0	0	0	0	0	1	0

- SVM and Kalman filter (SVMKF) (Sheibat-Othman et al., 2013): proposes a combined scheme for fault detection but does not meet detection times and marks NC on faults f_1, f_7, f_{10}.
- Residual SVM (RSVM) (Zeng et al., 2013): this scheme has hits and meets the detection times except for fault f_1.
- Standard interval observer (SIO) (Sanchez et al., 2015): the proposed scheme successfully detects all faults. However, its effectiveness relies heavily on the dynamic model's accuracy and fails to meet the required detection time for faults labeled as f_2 and f_7.
- Takagi–Sugeno interval observer (TSIO) (Pérez-Pérez et al., 2022): the proposed scheme demonstrates the capability to detect all faults. However, it does not accurately isolate faults f_4, f_7, and f_8.

The proposed method successfully diagnoses all faults within the required Time Diagnosis. The proposed method based on MANFIS and zonotopic observers verifies the congruence of the system estimates with the measurements at each step. All faults were correctly identified by incorporating an FSM. Nevertheless, it is important to note that this method is specifically designed for sequential faults, such as those commonly observed in wind turbines. For scenarios involving multiple simultaneous faults, it is necessary to implement alternative approaches to address these situations effectively.

7. Conclusions

This article introduces a hybrid wind turbine fault diagnosis approach combining machine learning techniques and TS zonotopic observers. The methodology involves a graphical process to obtain a set of MS, which considers the relationships between the Wind Turbine components and the measured variables. Two contributions are considered; the first involves identifying a collection of convex TS models based on the MS obtained by considering the MANFIS learning technique. All training data were obtained from fault-free scenarios. The second contribution was related to the design of zonotopic TS observers by considering the $\mathcal{H}_\infty$ criterion to guarantee robustness against uncertainty, disturbance, and noise. The approach considers both parametric uncertainty and disturbances as unknown but bounded. For fault diagnosis, a strategy is proposed that evaluates the generating residuals using a

Table 6
Comparison of the results achieved with preceding work.

Fault	T_D required	T_D obtained					
		TSZO	TSIO	AKNN	SVMKF	RSVM	SIO
f_1	$T_D < 10T_s$	$2T_s$	$2T_s$	NC	NC	NC	$3T_s$
f_2	$T_D < 10T_s$	T_s	$7T_s$	$17T_s$	$3T_s$	$6T_s$	$18T_s$
f_3	$T_D < 10T_s$	T_s	$2T_s$	$4T_s$	$22T_s$	T_s	$3T_s$
f_4	$T_D < 10T_s$	T_s	$2T_s$	$7T_s$	$44T_s$	$6T_s$	$3T_s$
f_5	$T_D < 10T_s$	$2T_s$	$2T_s$	$4T_s$	$11T_s$	$2T_s$	$3T_s$
f_6	$T_D < 10T_s$	T_s	$4T_s$	$13T_s$	$34T_s$	$6T_s$	$6T_s$
f_7	$T_D < 8T_s$	T_s	$5T_s$	NC	NC	$2T_s$	$375T_s$
f_8	$T_D < 100T_s$	T_s	$9T_s$	$11T_s$	$12T_s$	$2T_s$	$33T_s$
f_9	$T_D < 3T_s$	T_s	$2T_s$	$18T_s$	$35T_s$	$3T_s$	$3T_s$
f_{10}	$T_D < 50T_s$	$2T_s$	$3T_s$	$32T_s$	NC	$36T_s$	$3T_s$
Robustness		✓	✓	×	×	×	×

fault incidence matrix. The effectiveness of the method is tested on a certified wind turbine benchmark, encompassing various fault scenarios. Comparative analysis against multiple FD schemes demonstrates the method's applicability and satisfactory performance.

Some limitations of the present work are (i) the dependence of the analysis on the graph process since there is a possibility that the graph does not contain all relevant information or that some vital connection is omitted. Also, structural analysis based on GP requires many sensors and correct sensor placement to represent the system structure accurately; a lack of adequate sensors or incorrect sensor placement can affect the result. (ii) adaptability to other systems, implementing the proposed approach in other wind turbines or different systems may require retraining the MANFIS models and recalculating zonotope observer gains. This adaptability process may involve additional time and effort to tailor the methodology for specific system configurations and characteristics. However, it is essential to mention that the methodology presented here can be applied to other systems by following the steps mentioned on the document. These limitations will be addressed in future work and will also focus on developing prognosis systems to identify critical faults that could potentially harm the wind turbine system.

CRediT authorship contribution statement

Esvan-Jesús Pérez-Pérez: Conceptualization, Methodology, Data collection, Analysis, Manuscript writing. **Vicenç Puig:** Literature review, Data interpretation, Critical revisions. **Francisco-Ronay López-Estrada:** Conceptualization, Experimental design, Data analysis, Manuscript writing. **Guillermo Valencia-Palomo:** Statistical analysis, Manuscript drafting, Final approval of the version to be published. **Ildeberto Santos-Ruiz:** Data interpretation, Critical revisions, Manuscript editing. **Gloria Osorio-Gordillo:** Literature review, Manuscript revisions.

Declaration of competing interest

We wish to confirm that there are no known conflicts of interest associated with this publication (Robust fault diagnosis of wind turbines based on MANFIS and zonotopic observers) and there has been no significant financial support for this work that could have influenced its outcome.

Data availability

Data will be made available on request

Acknowledgments

This research has received support from the Consejo Nacional de Humanidades, Ciencias y Tecnologías (CONAHCYT), Mexico through the grant *Becas Nacionales* and by Tecnológico Nacional de México, Mexico under the program *Proyectos de Investigación Científica y Desarrollo Tecnológico e Innovación* and the international network *Red Internacional de Control y Cómputo Aplicado*, Mexico. All authors have read and approved the final version of the manuscript, and they take full responsibility for its accuracy and integrity. The order of authorship reflects the relative contributions and does not imply any hierarchy or seniority.

Appendix. Proof of Theorem 5.1

Proof. Consider the following quadratic Lyapunov function for system (29):

$$V(e(k)) = e(k)^T P e(k) > 0 \tag{A.1}$$

The increment function along the trajectory is:

$$\Delta V(e(k)) = V(e(k+1)) - V(e(k)) \tag{A.2}$$

The $\mathcal{H}_\infty$ criterion guarantees the asymptotic convergence of the estimation error and the robustness to disturbances, verifying the following dissipation inequality:

$$\Delta V(e(k)) + e(k)^T e(k) - \gamma^2 \varphi(k)^T \varphi(k) < 0 \tag{A.3}$$

Substituting (A.2) into (A.3) and using the dynamic equation of error (29), the following is obtained:

$$e(k)^T(\Phi_z^T P \Phi_z - P + I_n)e(k) + e(k)^T(\Phi_z^T P \Gamma_z)\varphi(k) + \varphi(k)^T(\Gamma_z^T P \Phi_z)e(k) + \varphi(k)^T(\Gamma_z^T P \Gamma_z - \gamma^2 I_n)\varphi(k) < 0 \tag{A.4}$$

Rewriting the previous expression in matrix form:

$$\begin{pmatrix} e(k)^T & \varphi(k)^T \end{pmatrix} \begin{pmatrix} \Phi_z^T P \Phi_z - P + I & \Phi_z^T P \Gamma_z \\ \Gamma_z^T P \Phi_z & \Gamma_z^T P \Gamma_z - \gamma^2 I \end{pmatrix} \begin{pmatrix} e(k) \\ \varphi(k) \end{pmatrix} \tag{A.5}$$

which can hold for any $\begin{pmatrix} e(k) \\ \varphi(k) \end{pmatrix}$ must be non-zero, if and only if

$$\begin{pmatrix} \Phi_z^T P \Phi_z - P + I & \Phi_z^T P \Gamma_z \\ \Gamma_z^T P \Phi_z & \Gamma_z^T P \Gamma_z - \gamma^2 I \end{pmatrix} < 0 \tag{A.6}$$

writing the condition as

$$\begin{pmatrix} -P + I & 0 \\ 0 & -\gamma^2 I \end{pmatrix} + \begin{pmatrix} \Phi_z^T P \Phi_z & \Phi_z^T P \Gamma_z \\ \Gamma_z^T P \Phi & \Gamma_z^T P \Gamma_z \end{pmatrix} < 0 \tag{A.7}$$

then, using the Schur complement, the following expression is obtained:

$$\begin{pmatrix} -P + I & 0 & \Phi_z^T P \\ 0 & -\gamma^2 I & \Gamma_z^T P \\ P \Phi_z & P \Gamma_z & -P \end{pmatrix} < 0 \tag{A.8}$$

replacing $\Phi_z = A_z - L_z C$ and $\Gamma_z = \begin{bmatrix} E_d & F_v & E_\delta \end{bmatrix}$, in (A.8), is haved:

$$\begin{pmatrix} -P+I & 0 & A_z^T P - C^T L_z^T P \\ \star & -\gamma^2 I & \begin{bmatrix} PE_d & -PL_z F_v & PE_\delta \end{bmatrix}^T \\ \star & \star & -P \end{pmatrix} < 0 \tag{A.9}$$

perform a change of variable in (A.9), such that $W_z = PL_z$, to transform this condition into an LMI, is obtained:

$$\begin{pmatrix} -P+I & 0 & A_z^T P - C^T W_z^T \\ \star & -\bar{\gamma} I & \begin{bmatrix} PE_d & -W_z F_v & PE_\delta \end{bmatrix}^T \\ \star & \star & -P \end{pmatrix} < 0 \tag{A.10}$$

extending the inequality in (A.10), we finally obtain as follows:

$$\begin{pmatrix} -P+I & 0 & 0 & 0 & A_z^T P - C^T W_z^T \\ \star & -\bar{\gamma} I & 0 & 0 & E_d^T P \\ \star & \star & -\bar{\gamma} I & 0 & F_v^T - W_z^T \\ \star & \star & \star & -\bar{\gamma} I & E_\delta^T P \\ \star & \star & \star & \star & -P \end{pmatrix} < 0 \tag{A.11}$$

By considering $\bar{\gamma} = \gamma^2$, sufficient LMI conditions are obtained. □

References

Alamo, T., Bravo, J. M., & Camacho, E. F. (2005). Guaranteed state estimation by zonotopes. *Automatica*, *41*(6), 1035–1043.

Barboni, A., Yang, G., Rezaee, H., & Parisini, T. (2022). On joint unknown input and sliding mode estimation. In *2022 European control conference* (pp. 969–974). IEEE.

Benmiloud, T. (2010). Multioutput adaptive neuro-fuzzy inference system. In *Proceedings of the 11th WSEAS international conference on nural networks and 11th WSEAS international conference on evolutionary computing and 11th WSEAS international conference on fuzzy systems* (pp. 94–98).

Blesa, J., Puig, V., & Bolea, Y. (2010). Fault detection using interval LPV models in an open-flow canal. *Control Engineering Practice*, *18*(5), 460–470.

Bougatef, Z., Abdelkrim, N., Aitouche, A., & Abdelkrim, M. N. (2020). Sensor fault detection and estimation based on UIO for LPV time delay systems using descriptor approach. In *Diagnosis, fault detection & tolerant control* (pp. 55–69). Springer.

Chen, B., Matthews, P. C., & Tavner, P. J. (2013). Wind turbine pitch faults prognosis using a-priori knowledge-based ANFIS. *Expert Systems with Applications*, *40*(17), 6863–6876.

Chen, J., & Patton, R. J. (2012). *Robust model-based fault diagnosis for dynamic systems, vol. 3*. Springer Science & Business Media.

Combastel, C. (2003). A state bounding observer based on zonotopes. In *2003 European control conference* (pp. 2589–2594). IEEE.

Le, V. T. H., Stoica, C., Alamo, T., Camacho, E. F., & Dumur, D. (2013). *Zonotopes: From guaranteed state-estimation to control*. John Wiley & Sons.

Li, H., Soares, C. G., & Huang, H.-Z. (2020). Reliability analysis of a floating offshore wind turbine using Bayesian networks. *Ocean Engineering*, *217*, Article 107827.

Liang, P., Wang, W., Yuan, X., Liu, S., Zhang, L., & Cheng, Y. (2022). Intelligent fault diagnosis of rolling bearing based on wavelet transform and improved ResNet under noisy labels and environment. *Engineering Applications of Artificial Intelligence*, *115*, Article 105269.

Liu, J., Wang, X., Wu, S., Wan, L., & Xie, F. (2023). Wind turbine fault detection based on deep residual networks. *Expert Systems with Applications*, *213*, Article 119102.

Liu, Z., & Zhang, L. (2020). A review of failure modes, condition monitoring and fault diagnosis methods for large-scale wind turbine bearings. *Measurement*, *149*, Article 107002.

McMorland, J., Flannigan, C., Carroll, J., Collu, M., McMillan, D., Leithead, W., & Coraddu, A. (2022). A review of operations and maintenance modelling with considerations for novel wind turbine concepts. *Renewable and Sustainable Energy Reviews*, *165*, Article 112581.

Odgaard, P. F., & Johnson, K. E. (2013). Wind turbine fault detection and fault tolerant control - An enhanced benchmark challenge. In *2013 American control conference* (pp. 4447–4452).

Pashazadeh, V., Salmasi, F. R., & Araabi, B. N. (2018). Data driven sensor and actuator fault detection and isolation in wind turbine using classifier fusion. *Renewable Energy*, *116*, 99–106.

Pérez-Pérez, E.-J., López-Estrada, F.-R., Puig, V., Valencia-Palomo, G., & Santos-Ruiz, I. (2022). Fault diagnosis in wind turbines based on ANFIS and Takagi–Sugeno interval observers. *Expert Systems with Applications*, Article 117698.

Perez-Zuniga, G., Chanthery, E., Travé-Massuyès, L., & Sotomayor, J. (2022). Near-optimal decentralized diagnosis via structural analysis. *IEEE Transactions on Systems, Man, and Cybernetics: Systems*, *52*(12), 7353–7365.

Pourasghar, M., Nguyen, A.-T., & Guerra, T.-M. (2022). Zonotopic observer designs for uncertain Takagi–Sugeno fuzzy systems. *Engineering Applications of Artificial Intelligence*, *114*, Article 105126.

Rahimilarki, R., Gao, Z., Zhang, A., & Binns, R. (2019). Robust neural network fault estimation approach for nonlinear dynamic systems with applications to wind turbine systems. *IEEE Transactions on Industrial Informatics*, *15*(12), 6302–6312.

Rajabi, S., Azari, M. S., Santini, S., & Flammini, F. (2022). Fault diagnosis in industrial rotating equipment based on permutation entropy, signal processing and multi-output neuro-fuzzy classifier. *Expert Systems with Applications*, *206*, Article 117754.

Sanchez, H., Escobet, T., Puig, V., & Odgaard, P. F. (2015). Fault diagnosis of an advanced wind turbine benchmark using interval-based ARRs and observers. *IEEE Transactions on Industrial Electronics*, *62*(6), 3783–3793.

Sato, M., & Marcos, A. (2020). Observer-based robust H_∞ fault-tolerant flight control: a design example and performance assessment. In *2020 59th IEEE conference on decision and control* (pp. 4706–4711). IEEE.

Sheibat-Othman, N., Othman, S., Benlahrache, M., & Odgaard, P. F. (2013). Fault detection and isolation in wind turbines using support vector machines and observers. In *2013 American control conference* (pp. 4459–4464). IEEE.

Song, J., & He, X. (2022). Model-based fault diagnosis of networked systems: A survey. *Asian Journal of Control*, *24*(2), 526–536.

Statistics GWEC (2023). *Global wind energy council*. Washington, DC, USA.

Su, Q., Wang, Z., Xu, J., Li, C., & Li, J. (2022). Fault detection for DC-DC converters using adaptive parameter identication. *Journal of the Franklin Institute*.

Sun, S., Hu, W., Liu, Y., Wang, T., & Chu, F. (2023). Matching contrastive learning: An effective and intelligent method for wind turbine fault diagnosis with imbalanced SCADA data. *Expert Systems with Applications*, *223*, Article 119891.

Sztyber, A., Ostasz, A., & Kościelny, J. M. (2015). Graph of a process—A new tool for finding model structures in a model-based diagnosis. *IEEE Transactions on Systems, Man, and Cybernetics: Systems*, *45*(7), 1004–1017.

Takagi, T., & Sugeno, M. (1985). Fuzzy identification of systems and its applications to modeling and control. *IEEE Transactions on Systems, Man, and Cybernetics, SMC-15*(1), 116–132.

Wang, Y., Puig, V., Cembrano, G., & Zhao, Y. (2021). Zonotopic fault detection observer for discrete-time descriptor systems considering- fault sensitivity. *International Journal of Systems Science*, *52*(1), 95–109.

Wang, Y., Puig, V., Xu, F., & Cembrano, G. (2019). Robust fault detection and isolation based on zonotopic unknown input observers for discrete-time descriptor systems. *Journal of the Franklin Institute*, *356*(10), 5293–5314.

Wang, J., Wang, Z., & Zhou, M. (2021). Adaptive event-triggered finite-frequency fault detection with zonotopic threshold analysis for LPV systems. *IEEE Transactions on Cybernetics*.

Zare, S., & Ayati, M. (2021). Simultaneous fault diagnosis of wind turbine using multichannel convolutional neural networks. *ISA Transactions*, *108*, 230–239.

Zeng, J., Lu, D., Zhao, Y., Zhang, Z., Qiao, W., & Gong, X. (2013). Wind turbine fault detection and isolation using support vector machine and a residual-based method. In *2013 American control conference* (pp. 3661–3666). IEEE.

Zhang, Z., Ma, M., Wang, H., Wang, H., Ma, W., & Zhang, X. (2021). A fault diagnosis method for photovoltaic module current mismatch based on numerical analysis and statistics. *Solar Energy*, *225*, 221–236.

Zhang, Y., Yu, K., Lei, Z., Ge, J., Xu, Y., Li, Z., Ren, Z., & Feng, K. (2023). Integrated intelligent fault diagnosis approach of offshore wind turbine bearing based on information stream fusion and semi-supervised learning. *Expert Systems with Applications*, *232*, Article 120854.